ACS APPLIED MATERIALS & INTERFACES

www.acsami.org

Research Article

Phosphonic Acid Modified ZnO Nanowire Sensors: Directing Reaction Pathway of Volatile Carbonyl Compounds

Chen Wang, Takuro Hosomi,* Kazuki Nagashima, Tsunaki Takahashi, Guozhu Zhang, Masaki Kanai, Hideto Yoshida, and Takeshi Yanagida*

Cite This: *ACS Appl. Mater. Interfaces* 2020, 12, 44265−44272

Read Online

ACCESS | Metrics & More | Article Recommendations | Supporting Information

ABSTRACT: Surface molecular transformations on nanoscale metal oxides are inherently complex, and directing those reaction pathways is still challenging but important for designing their various applications, including molecular sensing, catalysts, and others. Here, a rational strategy to direct a reaction pathway of volatile carbonyl compounds (nonanal: biomarker) on single-crystalline ZnO nanowire surfaces via molecular modification is demonstrated. The introduction of a methylphosphonic acid modification on the ZnO nanowire surface significantly alters the surface reaction pathway of nonanal via suppressing the detrimental aldol condensation reaction. This is directed by intentionally decreasing the probability of two neighboring molecular activations on the nanowire surface. Spectrometric measurements reveal the correlation between the suppression of the aldol condensation surface reaction and the improvement in the sensor performance. This tailored surface reaction pathway effectively reduces the operating temperature from 200 to 100 °C while maintaining the sensitivity. This is because the aldol condensation product ((*E*)-2-heptyl-2-undecenal) requires a higher temperature to desorb from the surface. Thus, the proposed facile strategy offers an interesting approach not only for the rational design of metal oxide sensors for numerous volatile carbonyl compounds but also for tailoring various surface reaction pathways on complex nanoscale metal oxides.

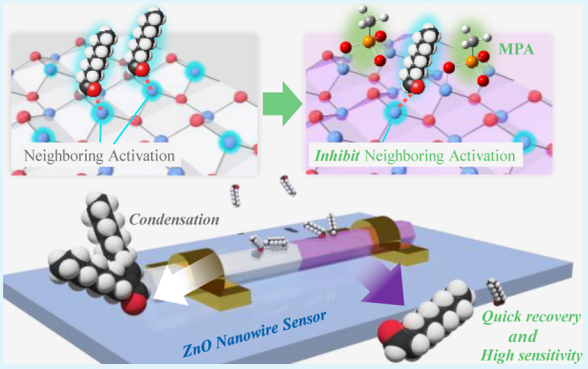

KEYWORDS: *metal oxide nanowires, molecular sensor, carbonyl compounds, molecular modification, directing reactions*

INTRODUCTION

Aliphatic aldehydes are most important chemical groups in the field of biosensing because of their ubiquities and informativities.[1,2] For example, nonanal, an aliphatic aldehyde with a carbon number of 9, can act as a disease marker because it is specifically found in the breath of lung cancer patients.[3,4] Therefore, the gas-phase aldehyde detection has received growing attention in the recent years by utilizing metal oxide semiconductor (MOS)-based electrical sensors.[5,6] On the other hand, the abundant reactivity of aliphatic aldehydes is often problematic for the MOS sensor applications. For instance, metal oxide surfaces are known to promote "aldol condensation" of aldehydes to yield much heavier products,[7−10] which can inhibit sensor recoveries. Thus, it has been strongly demanded to develop methodologies which selectively suppress such undesired reactions of aldehyde while allowing a desired reaction on metal oxide surfaces.

Directing a reaction pathway on a solid surface is still a challenging issue not only for the sensor applications but also in the heterogeneous reaction chemistry including heterogeneous catalysts.[11,12] Recently, operando observation techniques such as infrared (IR) spectroscopy, Raman spectroscopy, diffuse reflectance IR Fourier transform spectroscopy, and X-ray absorption spectroscopy have been developed to provide much insights into the reaction pathways at heterogeneous interfaces.[13−18] In addition, utilizing self-assembled monolayers on heterogeneous catalysts has attracted much interest because of their successful inhibitions of undesired reaction pathways.[19−28]

In this study, these designing concepts are applied to MOS sensors. Based on our previous spectrometric and spectroscopic observations of a metal oxide surface,[29] it was hypothesized that the undesired aldol condensation reaction can be suppressed by placing organic molecules on the surface. This is because the aldol condensation reaction is found to be promoted by a pair of spatially neighboring exposed Zn(II) ions on the metal oxide surface. Single-nanowire-based devices were fabricated to investigate the sensing properties using the proposed method (Figure 1). ZnO nanowires were selected

Received: June 9, 2020
Accepted: September 1, 2020
Published: September 1, 2020

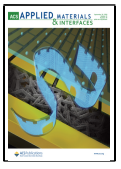

https://dx.doi.org/10.1021/acsami.0c10332
ACS Appl. Mater. Interfaces 2020, 12, 44265−44272

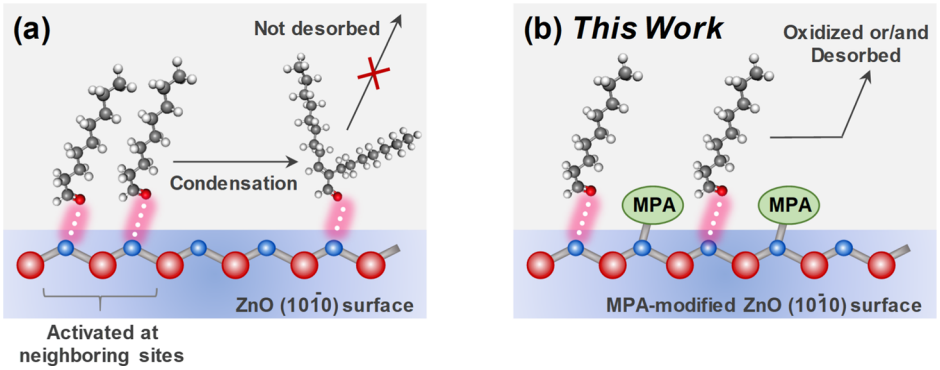

Figure 1. (a) Schematic image of the chemical transformation and desorption pathways of nonanal adsorbed on a ZnO nanowire. Surface-exposed Zn(II) ions on ZnO promotes aldol condensation of nonanals to yield a condensation product, which requires high temperature (>200 °C) to be desorbed. (b) Concept of this work. Surface-adsorbed MPA prevents nonanal from activating at the neighboring Zn(II) sites.

because ZnO has been extensively investigated for use in molecular sensors.[30−32] Phosphonic acid was used to cap the surface active sites because of their good covering ability on ZnO nanowires.[33,34] Methylphosphonic acid (MPA), which is the simplest phosphonic acid, was selected as the model molecule to prove the above-mentioned concepts. MPA has been reported to effectively modulate the catalytic activities of metal oxides (including ZnO) or metal/metal oxide surfaces.[35−44] Experimental results showed that the MPA modification on a single ZnO nanowire device successfully inhibited aldol condensation on the sensor surface and realized a decrease in the operating temperature for nonanal detection. Interestingly, the sensor response was not deteriorated by MPA modification and accomplished ultralow detection of nonanal, unlike the usual "surface passivation" approaches that often lower sensor sensitivity.[45] This is consistent with the temperature-programmed desorption mass spectrometry (TPD/MS) data, which does not show decrease of adsorption amount of nonanal, despite the MPA modification. This result has an interesting similarity to the previous studies of molecular-modified metal oxide catalysts, in which the catalytic activity was remarkably improved even though their surfaces were highly covered by molecules. Thus, these results not only experimentally demonstrate the effectiveness of our approach but also shed light on the fundamental chemistry which commonly underlies in the field of heterogeneous catalysts and metal oxide sensors.

EXPERIMENTAL SECTION

Growth of ZnO Nanowires. The hydrothermal method was utilized to grow ZnO nanowire arrays on Si(100) wafers. First, a 5 nm thick Ti buffer layer was sputtered on the Si substrate, and then a 100 nm thick ZnO thin film was sputtered as the seed layer. Zinc nitrate hexahydrate (25 mM) ($Zn(NO_3)_2{\cdot}6H_2O$, 99.0%), 25 mM hexamethylenetetramine ($(CH_2)_6N_4$, 99.0%), 2.5 mM polyethylenimine (number-average MW 1800, 50 wt % in H_2O), and ammonia ($NH_3{\cdot}6H_2O$, 6 mL, 28% in H_2O) were dissolved in deionized (DI) water (200 mL) sequentially. The preprepared substrate was dipped into the solution and kept at 95 °C for 9 h. After growth, the samples were rinsed with DI water and dried by N_2 flow. Then, the as-grown ZnO nanowires were annealed at 600 °C in air for 3 h.

Modification of MPA Molecules on ZnO Nanowires. MPA solutions with different concentrations (0.01, 0.1, 0.5, 1.0, 5.0, and 10 mM) were prepared by dissolving MPA powders (98%) in methanol at room temperature. The annealed ZnO nanowire array was first treated with O_2 plasma (150 W) for 10 min and then dipped into an MPA solution (2.5 mL) for 3 h at room temperature. Then, the samples were washed several times with methanol and heated at 100 °C for 10 min to remove residual organic molecules.

Characterization. X-ray diffraction (XRD) patterns were recorded with a Philips X'Pert diffractometer using a Cu Kα source (45 kV, 40 mA) at a wavelength of 1.54 Å. Scanning electron microscopy (SEM) images were obtained using a JEOL JSM-7610F microscope (accelerating voltage: 15.0 kV). Transmission electron microscopy (TEM) images were acquired using a JEOL ARM-200F. Energy-dispersive X-ray spectroscopy (EDXS) elemental mapping and spectra were investigated by SEM and TEM attachment. Fourier transform infrared (FT-IR) spectroscopy spectra were measured using a Nicolet iS50 FT-IR spectrometer (Thermo Fisher Scientific) equipped with a mercury−cadmium−telluride detector. The FT-IR spectra were scanned 300 times for each measurement, with a resolution of 4.0 cm^{-1} and a data point interval of 0.482 cm^{-1}.

Desorbed Gas Analysis Using Gas Chromatography−MS. Nonanal adsorption was carried out for bare ZnO nanowires and ZnO nanowires modified using various concentrations of MPA. The sample dimensions were 0.2 cm × 2.0 cm. Nonanal liquid (2 μL) was placed at the bottom of a 25 mL closed bottle and kept for 30 min to vaporize the nonanal gas. Prior to adsorption, the sample was pretreated at 250 °C for 30 min in vacuum using a sample degas system (VacPrep 061, Micromeritics) to remove residual molecules from the surrounding environment. Then, the sample was placed in a bottle filled with nonanal gas for a fixed time (30 s) and immediately transferred into the inlet port of the gas chromatography (GC)−MS instrument for further measurements. GC−MS (GC-MS-QP 2020, Shimadzu, Japan) with an OPTIC-4 inlet temperature control system was performed to analyze the desorbed compounds. The inlet temperature was maintained at 400 °C for 34 min and then immediately decreased to 35 °C. Supelco SLB-IL60 was used as the capillary column and heated from 40 to 280 °C at a rate of 10 °C/min. The temperature program is shown in detail in Figure S1.

Desorbed Gas Analysis by TPD/MS. The adsorption of the nonanal molecules was the same as that in the above process. GC−MS (GC-MS-QP 2020, Shimadzu, Japan) was used to collect the desorption spectrum using a capillary column (length: 1 m, internal diameter: 0.1 mm) without stationary phases to connect the inlet and the mass spectrometer unit. The sample temperature in the inlet port was controlled by a multishot pyrolyzer (EGA-PY-3030 D) and was changed from 35 to 500 °C at a heating rate of 0.5 °C/s (the detailed temperature program is shown in Figure S2). The change for m/z: 98 with an increase in the inlet temperature was monitored.

Fabrication of a Single-Nanowire Device and Sensing Measurements. The as-prepared nanowire arrays on the Si substrate were sonicated and dispersed in 2-propanol. Then, the dispersed nanowires were transferred onto an n-type silicon substrate capped with a 100 nm thick SiO_2 layer. Prior to transferring the nanowires onto the SiO_2/Si substrate, the macroelectrodes for contacting the electrical probes were fabricated using an electron-beam lithography (EBL) process. After EBL patterning, Pt (300 nm) nanogap

https://dx.doi.org/10.1021/acsami.0c10332
ACS Appl. Mater. Interfaces 2020, 12, 44265−44272

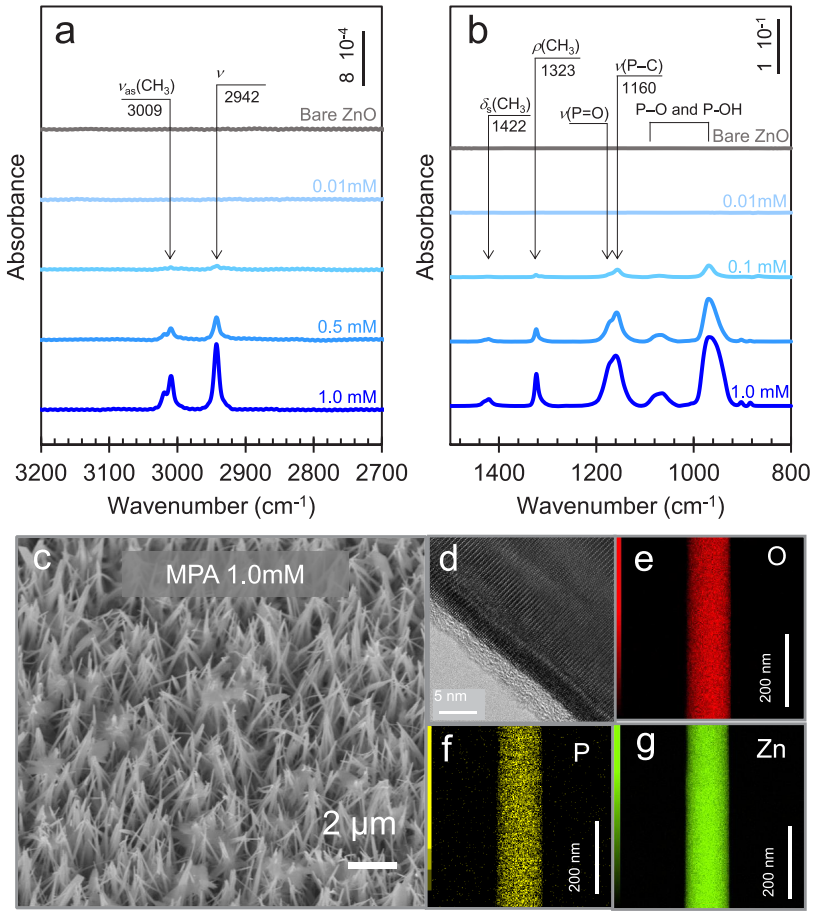

Figure 2. (a,b) FT-IR spectra of MPA-modified ZnO nanowires at various concentrations. (c) SEM image of the ZnO nanowire array after MPA modification (1.0 mM). (d) TEM image of an MPA-modified ZnO nanowire (1.0 mM). (e–g) Elemental distributions on an MPA-modified ZnO nanowire (1.0 mM) estimated by TEM–EDXS. Elemental distributions of the overall nanowire array are shown in Figure S5.

electrodes were deposited to contact the macroelectrodes and the nanowires. For all devices, nanowires with similar gaps (approximately 1.5 μm) and diameters (approximately 90 nm) were chosen to eliminate the possible distinction induced by the size of the nanowires. The sensing measurements were performed using a homemade testing system consisting of a gas supply system, a probe station with temperature control, and a semiconductor analyzer (Keithley 4200SCS) used to collect the electric signal. In addition, the sensing properties were investigated using a dynamic system. For these measurements, the gas flow rate was 0.25 mL/min, and the testing temperature was set to vary from 100 to 250 °C. The background gas was N_2 and the gas concentration was calibrated by GC–MS (the method is shown in detail in the Supporting Information and Figure S3). The response was defined as R_a/R_g, where R_a and R_g are the resistances of the sensor exposed to pure N_2 and the target gas, respectively. The recovery time was defined as the time required for the recovery of the resistance to 90% of R_a for the desorption process. Four or five devices were fabricated for each sample to obtain statistical data.

RESULTS AND DISCUSSION

The sensor fabrication process consists of the following steps: (1) growth of ZnO nanowire, (2) modification of MPA, and (3) sensor device fabrication and evaluation. First, ZnO nanowires were synthesized by a hydrothermal method. The obtained nanowires showed a single-crystalline wurtzite structure with a diameter of ~100 nm (Figure S4). Next, the nanowire was immersed in an MPA solution (1.0 mM) for 3 h, followed by dry N_2 flow, for the modification with a molecular layer. To confirm surface MPA modification, the FT-IR spectra of the modified ZnO nanowires were collected (Figure 2a,b). A set of the characteristic peaks of MPA (asymmetric stretching of CH_3 $\nu_{as}(CH_3)$: 3009 cm^{-1}, symmetric stretching of CH_3 $\nu_s(CH_3)$: 2942 cm^{-1}, symmetric umbrella bend of CH_3 $\delta_{as}(CH_3)$: 1422 cm^{-1}, rocking of CH_3 $\rho(CH_3)$: 1323 cm^{-1}, stretching of P═O ν(P═O): 1174 cm^{-1}, stretching of P–C ν(P–C): 1160 cm^{-1}, and ν(P–O) or ν(P–OH): 1067–970 cm^{-1})[46−48] is observed in the FT-IR spectra, confirming the adsorption of MPA on the ZnO surface. These values are in good agreement with the reported values of phosphonic acids bounded on ZnO, though the stretches in the P–O and P–OH regions are not able to be absolutely verified.[49] The peak intensities increase monotonically with increasing MPA concentration used in the immersion process, reflecting the increased surface coverage of MPA. The elemental distribution obtained by EDXS for the MPA-modified ZnO nanowire also supports the uniform distribution of MPA on the nanowire surface (Figure 2e–g). The geometrical and crystallographic structure of the ZnO nanowire did not show significant changes with the MPA modification in this concentration range (0.01–1.0 mM), as can be observed from the SEM (Figure 2c) and TEM (Figure 2d) images. Thus, these data confirmed that MPA molecules successfully modified the ZnO nanowires through the above-mentioned process. It should be noted that higher concentration of MPA (more than 5.0 mM) yields plate-like crystals of zinc methylphosphonate (Figures

https://dx.doi.org/10.1021/acsami.0c10332
ACS Appl. Mater. Interfaces 2020, 12, 44265–44272

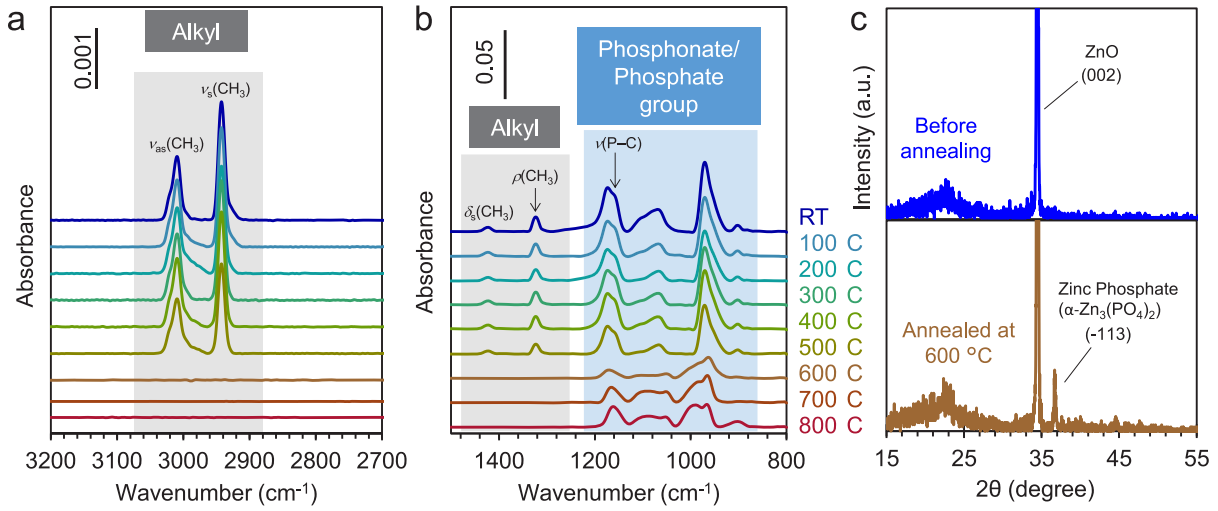

Figure 3. (a,b) Temperature-dependent FT-IR spectrum of MPA-modified ZnO nanowires (1.0 mM) after heating for 1 h in air at various temperatures. (c) XRD patterns of before (blue line) and after (brown line) 600 °C annealing of MPA-modified ZnO nanowires (1.0 mM).

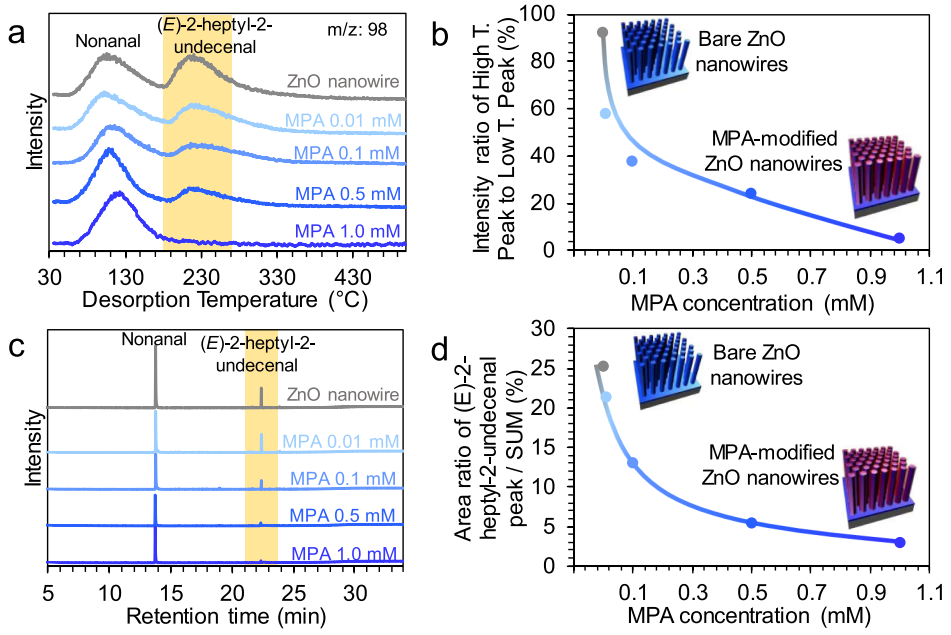

Figure 4. (a) Traces of TPD/MS profiles monitored at m/z = 98 as a function of desorption temperature. Each curve shows different concentrations of MPA used for modifying the ZnO nanowires. (b) Intensity ratio of the high-temperature peak and low-temperature peak in Figure 4a plotted vs the MPA concentrations. (c) GC−MS chromatograms of the desorption gas from the nonanal-adsorbed nanowires. (d) Area ratios of condensation product peaks against the summations of the peak areas of the condensation product and nonanal.

S6 and S7). Therefore, 1.0 mM condition was used in the following examinations.

Because MOS-based molecular sensors usually operate at high operating temperatures (≥100 °C), the thermal stability of the MPA modification was also explored prior to device fabrication. Figure 3a,b shows the FT-IR spectra of the MPA-modified ZnO nanowire obtained after heating for 1 h at various temperatures under atmospheric conditions. In the high-temperature region (>600 °C), the CH_3 and P−C peaks completely disappeared, whereas the peaks related to the P−O bond remained, implying that the thermal P−C bond cleavage occurred to form zinc phosphate. The XRD profile of the resultant nanowire (Figure 3c) also shows the formation of monoclinic α-$Zn_3(PO_4)_2$. By contrast, these CH_3 and P−C peaks were fully maintained below 500 °C. Based on these data, it is concluded that the thermal stability (up to 500 °C) of the MPA modification of the ZnO nanowires is sufficient for the use in MOS-based sensor applications.

The effects of MPA modification on the suppression of undesired molecular condensation on the ZnO surface were next investigated. For this purpose, the desorption temperatures and reaction products of an aliphatic aldehyde (nonanal) on the ZnO nanowires were evaluated by TPD/MS. MPA-modified ZnO nanowires were first exposed to a saturated vapor of nonanal to adsorb nonanal molecules and were then gradually heated to desorb the molecules on the ZnO surface. The desorption temperature and m/z patterns of the desorbed gas were analyzed by TPD/MS. Figure 4a shows the TPD/MS profiles of the gases desorbed from the nonanal-adsorbed ZnO nanowires modified by MPA at various

https://dx.doi.org/10.1021/acsami.0c10332
ACS Appl. Mater. Interfaces 2020, 12, 44265−44272

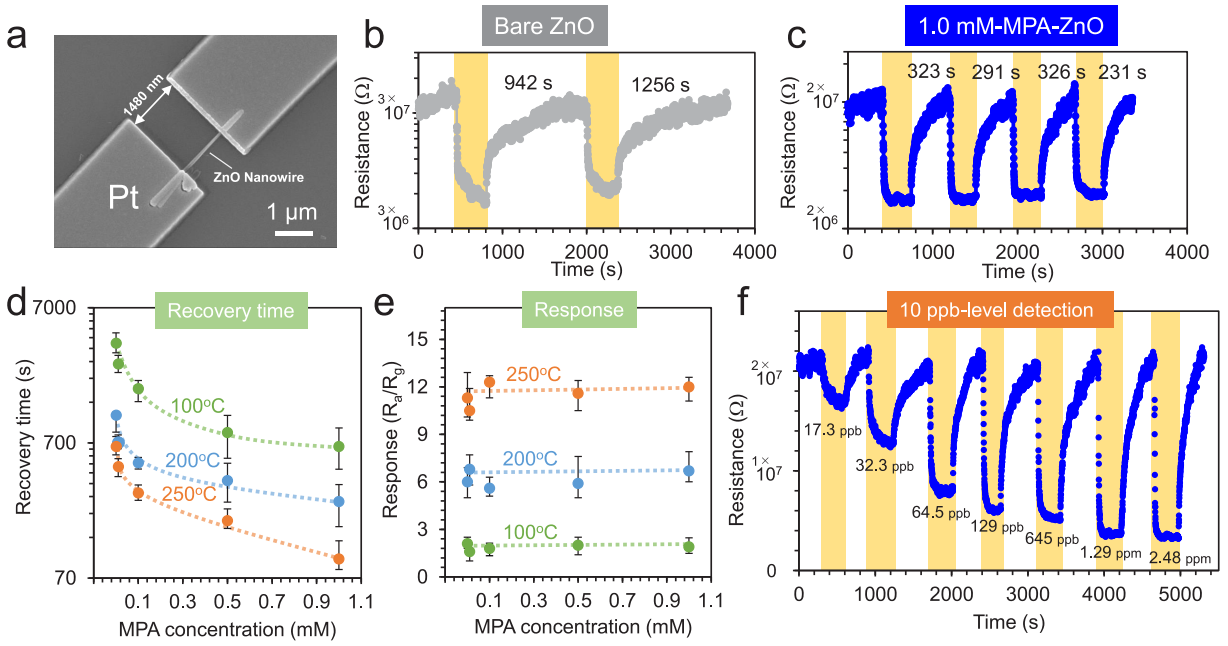

Figure 5. (a) SEM image of a typical single-nanowire device fabricated by the EBL technique. (b,c) Resistance trace of the sensor devices under alternating flow of pure N_2 (white region) and 2.48 ppm nonanal in N_2 (yellow region). The time denoted in the white region indicates the recovery time of each region. The recovery time is defined as the time required to obtain the original resistance value after the sample was exposed to nonanal for 200 s and then exposed to pure N_2 flow. A bare ZnO is used in (b), and an MPA-modified ZnO (1.0 mM) is used in (c). (d) Recovery time of the sensor at each temperature plotted vs MPA concentrations used for molecular modification. (e) Response (defined as R_a/R_g) at each temperature plotted vs MPA concentrations used for molecular modification. (f) Resistance trace of an MPA-modified ZnO sensor for various concentrations (from 17.3 ppb to 2.48 ppm) of nonanal in N_2 at 200 °C.

concentrations. In the profile for the bare ZnO nanowires, two distinct desorption peaks are observed. The low-temperature peak is assigned to nonanal, and the high-temperature peak (marked as yellow) is assigned to a condensation product of nonanal ((*E*)-2-heptyl-2-undecenal) based on a previous study.[29] Interestingly, this high-temperature peak gradually disappears with increasing MPA concentration used in the immersion process and almost completely disappears at 1.0 mM (Figure 4b). GC−MS analyses also show that the condensation product included in the desorbed gas from the ZnO nanowires decreases and almost disappears by increasing the MPA concentration (Figure 4c,d). These data indicate that the undesired condensation of aldehydes on the ZnO nanowire is effectively suppressed by the MPA modification. Figure 1 illustrates a plausible mechanism for the reaction suppression effect of the MPA. Our previous study revealed that the presence of neighboring Zn^{2+} ions exposed on ZnO is important for the acceleration of aldol condensation.[29] Bidentate adsorption of MPA is expected to partially cover these surface-exposed Zn^{2+} and decrease the number of neighboring Zn^{2+} ions, while leaving isolated Zn^{2+} sites available for adsorption of molecules. In fact, it should be noted that the amount of the adsorbed nonanal does not decrease even after MPA modification (Figure 4a). This indicates that the MPA modification does not hinder nonanal adsorption, probably because of its small steric hindrance. These data clearly demonstrate that MPA modification enables ZnO nanowires to adsorb and desorb aldehydes smoothly at lower temperatures. This feature is expected to lead to the fast recovery of MOS sensors under lower temperatures.

The effects of MPA modification on the molecular sensing properties were next evaluated (Figure 5). Single-nanowire devices were fabricated using a typical EBL technique (the detailed procedure is shown in the Experimental Section). Figure 5a shows the SEM image of a typical single ZnO nanowire device. All the devices show Ohmic *I*−*V* curves, as shown in Figure S8. The resistance (*R*) at a fixed voltage (1.0 V) and temperature (200 °C) was monitored under alternating flows of pure N_2 and 2.48 ppm nonanal in N_2. A typical current trace of a device using a bare ZnO nanowire is shown in Figure 5b. A fast response to nonanal gas is observed, and the resistance value (R_g) is reduced to approximately 20% of the original value (R_a). However, a long time (about 1000 s) is required to again reach the original resistance value after exposure to pure N_2 gas. This slow recovery is considered to be due to the surface residual condensation product because the desorption temperature of this product (approximately 230 °C, Figure 4a) is higher than the current working temperature of the sensor (200 °C). By contrast, the recovery time for a device using MPA-modified ZnO nanowires is much lower (Figure 5c). The recovery time decreased monotonically with increasing MPA concentration (Figures 5d and S9) and was 5 times lower than that of the bare ZnO nanowire for an MPA concentration of 1.0 mM, reflecting the suppression of surface condensation. Interestingly, despite the suppression of the surface reaction, the response (R_a/R_g) did not decrease in this concentration range (Figure 5e). These good response/recovery characteristics were maintained even under ultralow concentrations as low as 17.3 ppb (Figure 5f). These trends are in good agreement with the results of the above-mentioned TPD/MS analyses, confirming our hypothesis that the suppression of undesired condensation reactions is important for obtaining good sensor properties. Moreover, this recovery time shortening effect is observed over a wide range of temperatures (100−250 °C), as shown in Figure 5c,d. In other words, the MPA modification enables the sensor to operate at

https://dx.doi.org/10.1021/acsami.0c10332
ACS Appl. Mater. Interfaces 2020, 12, 44265−44272

lower temperatures without negatively affecting their recovery times. These results clearly demonstrate the effectiveness of our strategy of tailoring surface reactions by molecular modification for the design of molecular sensor performance.

CONCLUSIONS

In summary, an effective strategy for designing the performance characteristics of ZnO nanowire-based molecular sensors has been successfully demonstrated. Based on the reaction mechanism of the target molecule (nonanal) on metal oxide surfaces, an appropriate surface modification molecule (MPA) was designed to selectively suppress the undesired reaction (aldol condensation) that negatively affects the recovery time. The molecular modification and its effect were examined in detail using SEM, TEM, EDXS, FT-IR, and TPD/MS. These analyses showed that the reaction pathway of the target molecule was tailored as intended, and this tailoring enabled ZnO nanowires to adsorb and desorb molecules smoothly at lower temperatures. The investigation of the molecular sensor properties proved that the suppression of the condensation reaction is an effective approach for improving the sensor performance. By using the MPA-modified ZnO nanowires, the recovery time of the molecular sensor was decreased drastically, while their response was maintained over a wide range of temperatures. This property is quite useful for lowering the operating temperature of the sensor, which is a key challenge for MOS-based molecular sensors. A further development of the new strategy for the design of sensor performance presented here will provide more highly controlled MOS-based molecular sensors.

ASSOCIATED CONTENT

Supporting Information

The Supporting Information is available free of charge at https://pubs.acs.org/doi/10.1021/acsami.0c10332.

Temperature programs of GC-MS and TPD/MS; calibration curves of GC−MS; SEM and TEM images of ZnO nanowires; SEM images of MPA-modified ZnO nanowires; XRD profiles of MPA-modified ZnO nanowires; EDXS mappings of ZnO nanowires; and current−voltage (I−V) curves of single-nanowire devices (PDF)

AUTHOR INFORMATION

Corresponding Authors

Takuro Hosomi − *Department of Applied Chemistry, Graduate School of Engineering, The University of Tokyo, Tokyo 113-8656, Japan; Japan Science and Technology Agency (JST)-PRESTO, Kawaguchi, Saitama 332-0012, Japan;* orcid.org/0000-0002-5649-6696; Email: t-hosomi@g.ecc.u-tokyo.ac.jp

Takeshi Yanagida − *Institute for Materials Chemistry and Engineering, Kyushu University, Kasuga, Fukuoka 816-8580, Japan; Department of Applied Chemistry, Graduate School of Engineering, The University of Tokyo, Tokyo 113-8656, Japan;* orcid.org/0000-0003-4837-5701; Phone: +81-3-5841-3840; Email: yanagida@g.ecc.u-tokyo.ac.jp; Fax: +81-3-5841-3862

Authors

Chen Wang − *Institute for Materials Chemistry and Engineering, Kyushu University, Kasuga, Fukuoka 816-8580, Japan;* orcid.org/0000-0002-5678-5287

Kazuki Nagashima − *Department of Applied Chemistry, Graduate School of Engineering, The University of Tokyo, Tokyo 113-8656, Japan; Japan Science and Technology Agency (JST)-PRESTO, Kawaguchi, Saitama 332-0012, Japan;* orcid.org/0000-0003-0180-816X

Tsunaki Takahashi − *Department of Applied Chemistry, Graduate School of Engineering, The University of Tokyo, Tokyo 113-8656, Japan; Japan Science and Technology Agency (JST)-PRESTO, Kawaguchi, Saitama 332-0012, Japan;* orcid.org/0000-0002-2840-8038

Guozhu Zhang − *Department of Applied Chemistry, Graduate School of Engineering, The University of Tokyo, Tokyo 113-8656, Japan*

Masaki Kanai − *Department of Applied Chemistry, Graduate School of Engineering, The University of Tokyo, Tokyo 113-8656, Japan*

Hideto Yoshida − *The Institute of Scientific and Industrial Research, Osaka University, Ibaraki, Osaka 567-0047, Japan*

Complete contact information is available at: https://pubs.acs.org/10.1021/acsami.0c10332

Author Contributions

Sample fabrication, spectroscopic measurements, and sensor evaluations were performed by C.W. TEM measurements were performed by H.Y. Characterizations of the nanowire and molecular functionalization states by the obtained data were conducted by C.W., T.H., and K.N. The molecular adsorption and desorption behaviors were discussed by C.W., T.H., K.N., T.T., G.Z., M.K., and T.Y. T.H. and T.Y. wrote this manuscript and C.W., K.N., T.T., G.Z., M.K., and H.Y. contributed to improve the manuscript. All the authors contributed to manuscript preparation and approved the final version of the manuscript.

Notes

The authors declare no competing financial interest.

ACKNOWLEDGMENTS

This work was supported by KAKENHI (grant nos. JP17H04927, JP18H01831, JP18H05243, and JP18KK0112). T.H. was supported by JST PRESTO, Japan (grant no. JPMJPR19T8). T.H., K.N., T.T., and T.Y. were supported by JST CREST, Japan (grant no. JPJSBP120187207), JST Mirai R&D. T.Y. and K.N. were supported by the CAS−JSPS Joint Research Projects (grant no. GJHZ1891). This work was performed under the Cooperative Research Program of "Network Joint Research Center for Materials and Devices", "Dynamic Alliance for Open Innovation Bridging Human, Environment and Materials", and the MEXT Project of "Integrated Research Consortium on Chemical Sciences".

REFERENCES

(1) Mallya, A. N.; Ramamurthy, P. C. Organic Molecule Based Sensor for Aldehyde Detection. *Sensing Technology: Current Status and Future Trends III*; Mason, A., Mukhopadhyay, S. C., Jayasundera, K. P., Eds.; Springer International Publishing: Cham, 2015.

(2) Laghrib, F.; Lahrich, S.; Mhammedi, M. A. E. Review—Recent Advances in Direct and Indirect Methods for Sensing Carbonyl Compounds Aldehydes in Environment and Foodstuffs. *J. Electrochem. Soc.* **2019**, *166*, B1543−B1551.

(3) Das, S.; Pal, M. Review—Non-Invasive Monitoring of Human Health by Exhaled Breath Analysis: A Comprehensive Review. *J. Electrochem. Soc.* **2020**, *167*, 037562.

(4) Zhou, X.; Xue, Z.; Chen, X.; Huang, C.; Bai, W.; Lu, Z.; Wang, T. Nanomaterial-Based Gas Sensors Used for Breath Diagnosis. *J. Mater. Chem. B* **2020**, *8*, 3231−3248.
(5) Konvalina, G.; Haick, H. Sensors for Breath Testing: From Nanomaterials to Comprehensive Disease Detection. *Acc. Chem. Res.* **2014**, *47*, 66−76.
(6) Spinelle, L.; Gerboles, M.; Kok, G.; Persijn, S.; Sauerwald, T. Review of Portable and Low-Cost Sensors for the Ambient Air Monitoring of Benzene and Other Volatile Organic Compounds. *Sensors* **2017**, *17*, 1520.
(7) Ji, W.; Chen, Y.; Kung, H. H. Vapor Phase Aldol Condensation of Acetaldehyde on Metal Oxide Catalysts. *Appl. Catal., A* **1997**, *161*, 93−104.
(8) Mäki-Arvela, P.; Shcherban, N.; Lozachmeur, C.; Eränen, K.; Aho, A.; Smeds, A.; Kumar, N.; Peltonen, J.; Peurla, M.; Russo, V.; Volcho, K. P.; Murzin, D. Y. Aldol Condensation of Cyclopentanone with Valeraldehyde Over Metal Oxides. Catal. *Letters* **2019**, *149*, 1383−1395.
(9) Singh, M.; Zhou, N.; Paul, D. K.; Klabunde, K. J. IR Spectral Evidence of Aldol Condensation: Acetaldehyde Adsorption over TiO_2 Surface. *J. Catal.* **2008**, *260*, 371−379.
(10) Idriss, H.; Barteau, M. A. Selectivity and Mechanism Shifts in the Reactions of Acetaldehyde on Oxidized and Reduced TiO2(001) Surfaces. Catal. *Letters* **1996**, *40*, 147−153.
(11) Burueva, D. B.; Kovtunova, L. M.; Bukhtiyarov, V. I.; Kovtunov, K. V.; Koptyug, I. V. Single-Site Heterogeneous Catalysts: From Synthesis to NMR Signal Enhancement. *Chem.—Eur. J.* **2019**, *25*, 1420−1431.
(12) Balasubramanian, T. S.; Vijayamohanan, K.; Shukla, A. K. Mechanisms of the Discharge of Porous-Iron Electrodes in Alkaline Medium. *J. Appl. Electrochem.* **1993**, *23*, 947−950.
(13) Rodriguez, J. A.; Hanson, J. C.; Chupas, P. J. *In-Situ Characterization of Heterogeneous Catalysts*; Wiley−Blackwell: Chichester, 2013.
(14) James, H. F. *In-Situ Spectroscopy in Heterogeneous Catalysis*; Wiley-VCH: Weinheim, 2002.
(15) Zaera, F. New Advances in the Use of Infrared Absorption Spectroscopy for the Characterization of Heterogeneous Catalytic Reactions. *Chem. Soc. Rev.* **2014**, *43*, 7624−7663.
(16) Zhang, Y.; Fu, D.; Xu, X.; Sheng, Y.; Xu, J.; Han, Y.-f. Application of Operando Spectroscopy on Catalytic Reactions. *Curr. Opin. Chem. Eng.* **2016**, *12*, 1−7.
(17) Gurlo, A.; Riedel, R. In Situ and Operando Spectroscopy for Assessing Mechanisms of Gas Sensing. *Angew. Chem., Int. Ed.* **2007**, *46*, 3826−3848.
(18) Harks, P. P. R. M. L.; Mulder, F. M.; Notten, P. H. L. In Situ Methods for Li-Ion Battery Research: A Review of Recent Developments. *J. Power Sources* **2015**, *288*, 92−105.
(19) Marshall, S. T.; O'Brien, M.; Oetter, B.; Corpuz, A.; Richards, R. M.; Schwartz, D. K.; Medlin, J. W. Controlled Selectivity for Palladium Catalysts Using Self-Assembled Monolayers. *Nat. Mater.* **2010**, *9*, 853−858.
(20) Wu, B.; Huang, H.; Yang, J.; Zheng, N.; Fu, G. Selective Hydrogenation of *α,β*-Unsaturated Aldehydes Catalyzed by Amine-Capped Platinum-Cobalt Nanocrystals. *Angew. Chem., Int. Ed.* **2012**, *51*, 3440−3443.
(21) Kwon, S. G.; Krylova, G.; Sumer, A.; Schwartz, M. M.; Bunel, E. E.; Marshall, C. L.; Chattopadhyay, S.; Lee, B.; Jellinek, J.; Shevchenko, E. V. Capping Ligands as Selectivity Switchers in Hydrogenation Reactions. *Nano Lett.* **2012**, *12*, 5382−5388.
(22) Kahsar, K. R.; Schwartz, D. K.; Medlin, J. W. Control of Metal Catalyst Selectivity through Specific Noncovalent Molecular Interactions. *J. Am. Chem. Soc.* **2014**, *136*, 520−526.
(23) Schrader, I.; Warneke, J.; Backenköhler, J.; Kunz, S. Functionalization of Platinum Nanoparticles with l -Proline: Simultaneous Enhancements of Catalytic Activity and Selectivity. *J. Am. Chem. Soc.* **2015**, *137*, 905−912.
(24) Pang, S. H.; Schoenbaum, C. A.; Schwartz, D. K.; Medlin, J. W. Directing Reaction Pathways by Catalyst Active-Site Selection Using Self-Assembled Monolayers. *Nat. Commun.* **2013**, *4*, 2448.
(25) Schoenbaum, C. A.; Schwartz, D. K.; Medlin, J. W. Controlling the Surface Environment of Heterogeneous Catalysts Using Self-Assembled Monolayers. *Acc. Chem. Res.* **2014**, *47*, 1438−1445.
(26) Jia, X.; Ma, J.; Xia, F.; Xu, Y.; Gao, J.; Xu, J. Carboxylic Acid-Modified Metal Oxide Catalyst for Selectivity-Tunable Aerobic Ammoxidation. *Nat. Commun.* **2018**, *9*, 933.
(27) Jia, X.; Ma, J.; Xia, F.; Gao, M.; Gao, J.; Xu, J. Switching Acidity on Manganese Oxide Catalyst with Acetylacetones for Selectivity-Tunable Amines Oxidation. *Nat. Commun.* **2019**, *10*, 2338.
(28) Chen, G.; Xu, C.; Huang, X.; Ye, J.; Gu, L.; Li, G.; Tang, Z.; Wu, B.; Yang, H.; Zhao, Z.; Zhou, Z.; Fu, G.; Zheng, N. Interfacial Electronic Effects Control the Reaction Selectivity of Platinum Catalysts. *Nat. Mater.* **2016**, *15*, 564−569.
(29) Wang, C.; Hosomi, T.; Nagashima, K.; Takahashi, T.; Zhang, G.; Kanai, M.; Zeng, H.; Mizukami, W.; Shioya, N.; Shimoaka, T.; Tamaoka, T.; Yoshida, H.; Takeda, S.; Yasui, T.; Baba, Y.; Aoki, Y.; Terao, J.; Hasegawa, T.; Yanagida, T. Rational Method of Monitoring Molecular Transformations on Metal-Oxide Nanowire Surfaces. *Nano Lett.* **2019**, *19*, 2443−2449.
(30) Spencer, M. J. S. Gas Sensing Applications of 1D-Nanostructured Zinc Oxide: Insights from Density Functional Theory Calculations. *Prog. Mater. Sci.* **2012**, *57*, 437−486.
(31) Katwal, G.; Paulose, M.; Rusakova, I. A.; Martinez, J. E.; Varghese, O. K. Rapid Growth of Zinc Oxide Nanotube−Nanowire Hybrid Architectures and Their Use in Breast Cancer-Related Volatile Organics Detection. *Nano Lett.* **2016**, *16*, 3014−3021.
(32) Ahn, M.-W.; Park, K.-S.; Heo, J.-H.; Kim, D.-W.; Choi, K. J.; Park, J.-G. On-Chip Fabrication of ZnO-Nanowire Gas Sensor with High Gas Sensitivity. *Sens. Actuators, B* **2009**, *138*, 168−173.
(33) Zhang, B.; Kong, T.; Xu, W.; Su, R.; Gao, Y.; Cheng, G. Surface Functionalization of Zinc Oxide by Carboxyalkylphosphonic Acid Self-Assembled Monolayers. *Langmuir* **2010**, *26*, 4514−4522.
(34) Ito, D.; Jespersen, M. L.; Hutchison, J. E. Selective Growth of Vertical ZnO Nanowire Arrays Using Chemically Anchored Gold Nanoparticles. *ACS Nano* **2008**, *2*, 2001−2006.
(35) Ellis, L. D.; Trottier, R. M.; Musgrave, C. B.; Schwartz, D. K.; Medlin, J. W. Controlling the Surface Reactivity of Titania via Electronic Tuning of Self-Assembled Monolayers. *ACS Catal.* **2017**, *7*, 8351−8357.
(36) Van Cleve, T.; Underhill, D.; Veiga Rodrigues, M.; Sievers, C.; Medlin, J. W. Enhanced Hydrothermal Stability of γ-Al_2O_3 Catalyst Supports with Alkyl Phosphonate Coatings. *Langmuir* **2018**, *34*, 3619−3625.
(37) Coan, P. D.; Ellis, L. D.; Griffin, M. B.; Schwartz, D. K.; Medlin, J. W. Enhancing Cooperativity in Bifunctional Acid-Pd Catalysts with Carboxylic Acid-Functionalized Organic Monolayers. *J. Phys. Chem. C* **2018**, *122*, 6637−6647.
(38) Zhang, J.; Ellis, L. D.; Wang, B.; Dzara, M. J.; Sievers, C.; Pylypenko, S.; Nikolla, E.; Medlin, J. W. Control of Interfacial Acid-Metal Catalysis with Organic Monolayers. *Nat. Catal.* **2018**, *1*, 148−155.
(39) Ellis, L. D.; Ballesteros-Soberanas, J.; Schwartz, D. K.; Medlin, J. W. Effects of Metal Oxide Surface Doping with Phosphonic Acid Monolayers on Alcohol Dehydration Activity and Selectivity. *Appl. Catal., A* **2019**, *571*, 102−106.
(40) Ballesteros-Soberanas, J.; Ellis, L. D.; Medlin, J. W. Effects of Phosphonic Acid Monolayers on the Dehydration Mechanism of Aliphatic Alcohols on TiO2. *ACS Catal.* **2019**, *9*, 7808−7816.
(41) Jenkins, A. H.; Musgrave, C. B.; Medlin, J. W. Enhancing Au/TiO2 Catalyst Thermostability and Coking Resistance with Alkyl Phosphonic-Acid Self-Assembled Monolayers. *ACS Appl. Mater. Interfaces* **2019**, *11*, 41289−41296.
(42) Queffélec, C.; Petit, M.; Janvier, P.; Knight, D. A.; Bujoli, B. Surface Modification Using Phosphonic Acids and Esters. *Chem. Rev.* **2012**, *112*, 3777−3807.

https://dx.doi.org/10.1021/acsami.0c10332
ACS Appl. Mater. Interfaces 2020, 12, 44265−44272

(43) Paniagua, S. A.; Giordano, A. J.; Smith, O. L.; Barlow, S.; Li, H.; Armstrong, N. R.; Pemberton, J. E.; Brédas, J.-L.; Ginger, D.; Marder, S. R. Phosphonic Acids for Interfacial Engineering of Transparent Conductive Oxides. *Chem. Rev.* **2016**, *116*, 7117−7158.
(44) Cattani-Scholz, A. Functional Organophosphonate Interfaces for Nanotechnology: A Review. *ACS Appl. Mater. Interfaces* **2017**, *9*, 25643−25655.
(45) Mwathe, P. M.; Musembi, R.; Munji, M.; Odari, B.; Munguti, L.; Ntilakigwa, A.; Mwabora, J.; Njoroge, W.; Aduda, B.; Muthoka, B. Surface Passivation Effect on CO2 Sensitivity of Spray Pyrolysis Deposited Pd-F: SnO2 Thin Film Gas Sensor. *Adv. Mater.* **2014**, *3*, 38−44.
(46) Long, D. A. Infrared and Raman Characteristic Group Frequencies. Tables and Charts George Socrates John Wiley and Sons, Ltd, Chichester, Third Edition, 2001. *J. Raman Spectrosc.* **2004**, *35*, 905.
(47) Schuschke, C.; Schwarz, M.; Hohner, C.; Silva, T. N.; Fromm, L.; Döpper, T.; Görling, A.; Libuda, J. Phosphonic Acids on an Atomically Defined Oxide Surface: The Binding Motif Changes with Surface Coverage. *J. Phys. Chem. Lett.* **2018**, *9*, 1937−1943.
(48) Schuschke, C.; Schwarz, M.; Hohner, C.; Silva, T. N.; Libuda, J. Phosphonic Acids on Well-Ordered CoO Surfaces: The Binding Motif Depends on the Surface Structure. *J. Phys. Chem. C* **2018**, *122*, 16221−16233.
(49) Quiñones, R.; Rodriguez, K.; Iuliucci, R. J. Investigation of Phosphonic Acid Surface Modifications on Zinc Oxide Nanoparticles under Ambient Conditions. *Thin Solid Films* **2014**, *565*, 155−164.

https://dx.doi.org/10.1021/acsami.0c10332
ACS Appl. Mater. Interfaces 2020, 12, 44265−44272